

# Improved quantitative analysis of hard coatings by radiofrequency glow discharge optical emission spectrometry (rf-GD-OES)

Richard Payling,<sup>\*a</sup> Max Aeberhard<sup>b</sup> and Daniel Delfosse<sup>c</sup>

<sup>a</sup>Surface Analytical, 8 Donaldson Street, Port Kembla NSW 2505, Australia.

E-mail: Designer@TheSpectroscopyNet.com

<sup>b</sup>EMPA, Fuerwerkerstrasse 39, CH-3602 Thun, Switzerland

<sup>c</sup>Mathys Medical Ltd., Orthopaedics, Güterstrasse 5, CH-2544 Bettlach, Switzerland

Received 18th September 2000, Accepted 6th November 2000

First published as an Advance Article on the web 18th December 2000

Quantitative depth profiles are presented for a variety of hard coatings on tool steel. The coatings include TiN, TiC, TiCN and Cr<sub>7</sub>C<sub>3</sub> coatings, produced in a commercial furnace by chemical vapour deposition (CVD), and TiAlN, CrN and MoS<sub>2</sub>+Ti coatings, prepared in a laboratory coater by physical vapour deposition (PVD). The profiles were obtained using rf-GD-OES and are the first to use a dc bias voltage correction and a hydrogen correction. These corrections involve a term called the 'inverse relative emission yield' and are simple functions of the dc bias voltage and hydrogen signal. These corrections mean bulk and coated samples with different electrical characteristics can be combined in a single calibration. The correct quantitative depth profile can now be obtained even in the presence of significant amounts of hydrogen in the coating.

## Introduction

Hard coatings, including TiN, TiC, TiCN and TiAlN, are of major commercial interest. They reduce the wear, friction and corrosion of tools and components, and provide decorative finishes. Commonly, these coatings are prepared by chemical vapour deposition (CVD) or by physical vapour deposition (PVD). CVD relies on circulating gas, rather than the line-of-sight of ion-beam techniques, and so is well suited to coating complex shapes.<sup>1</sup> PVD includes reactive magnetron sputtering, ion plating and arc evaporation.<sup>2</sup>

Glow discharge optical emission spectrometry (GD-OES) provides a rapid and sensitive depth profile analysis of these coatings.<sup>3,4</sup> GD-OES therefore has much to offer this industry, by assisting in the development of new coatings and the testing of new processes, and in quality assurance and production problem solving. For these applications GD-OES has major advantages over competing techniques, such as Auger electron spectroscopy (AES), secondary-ion mass spectroscopy (SIMS) and energy dispersive analysis (EDX), in its unique combination of great speed, sensitivity and ease of quantification.<sup>5</sup>

The first qualitative GD-OES depth profiles of these coatings appeared in 1984<sup>6</sup> and the first quantitative depth profiles in 1986.<sup>7</sup> Since then the number of publications using quantitative GD-OES analysis of hard coatings has continued to grow.<sup>8</sup> Recent quantitative work includes: TiCN,<sup>9,10</sup> (Ti, Fe)N,<sup>11</sup> TiAlN,<sup>12,13</sup> diamond-like carbon,<sup>14</sup> TiN,<sup>15</sup> WC/C<sup>16</sup> and (Ti, Al, Zr)N.<sup>17</sup> Wänstrand and co-workers studied a variety of Ti and W carbides and nitrides but were unable to get quantitative GD-OES analysis because of hydrogen in the coatings interfering with measured intensities.<sup>18,19</sup> Their GD-OES results were provided by Bengtson,<sup>18</sup> and this is probably the first published reference to this problem.

We present here an improved method for quantitative GD-OES depth profiles of hard coatings. This is the first method to account for all known variables in the plasma, notably the electrical plasma parameters, pressure and the hydrogen effect. While the method is applicable to direct current (dc) operation, it is aimed principally at radiofrequency (rf) operation. All our results presented here were obtained with an rf powered glow discharge source.

In GD-OES, the plasma pressure and electrical parameters, such as current and voltage or power, are all inter-related. It is not normally possible to control all of these parameters during calibration and analysis. Either the electrical parameters are fixed and the pressure varied or the pressure is held constant and one electrical parameter varied. In rf-GD-OES, a common practice, and the one adopted here, is to keep the pressure and applied power constant. In this case, the impedance (or the ratio of voltage to current) varies from sample to sample. Whichever method is employed, the varying parameter can influence the measured intensity and this effect needs to be corrected.

In GD-OES, the purity of the low-pressure glow discharge plasma is largely determined by the purity of the argon used both to flush the source and as the plasma gas. Sputtered material from the source typically constitutes only about 0.1% of the plasma density. Recent work by Bengtson and Hänström<sup>20</sup> and Hodoroaba *et al.*<sup>21,22</sup> has shown that hydrogen contents in the plasma as low as 0.01% can have a significant effect on the intensities of analyte emission lines measured in the plasma. Hydrogen sputtered from samples containing significant amounts of hydrogen are therefore capable of reaching or exceeding this level, and so will alter the intensities measured with these samples. This constitutes a serious problem in the analysis of hard coatings containing variable amounts of hydrogen.

## Experimental

The samples used for calibration included bulk samples: six certified reference materials (CRMs), one reference material, one compressed powder, and four CVD coated tool steels (TiC, TiN, TiCN, Cr<sub>7</sub>C<sub>3</sub>). The samples used for quantitative depth profiling analysis were the four CVD coated tool steels used in the calibration plus four sputter deposited coatings on spring steel.

The CRMs used were SRM 1265a (nearly pure iron, from National Institute of Standards and Technology, NIST, USA), JK41-1N (Coronite Fe-Ti alloy with N 6.9%, Swedish Institute for Metals Research, Sweden), SS487/1 (high speed tool steel

with C 1%, Cr 3.9%, Mo 9.4%, from Bureau of Analysed Samples, UK), 1203 (Maraging 250 steel with Ni 18.4%, Mo 4.9%, from Certech, USA), BS80D (austenitic stainless-steel with Cr 17.2%, Ni 8.7%, from MBH Analytical, UK), and SRM 1169 (lead-bearing steel with 0.3% S, from NIST, USA).

The reference material was 550/3 (Ti alloy with Mo 4.2%, Al 4.2%, from Claxton, USA). The powder sample was high purity TiN powder hot-isostatically pressed.

The steel used for the CVD coatings was X155CrVMo12-1 (tool steel with C 1.5%, Cr 11–12%, Mo 0.6–0.8%, from Böhler Stahl, Switzerland). The steel arrived as a bar of 45.8 mm diameter. The bar was cut with a saw into disks of 6 mm thickness. The disks were then ground flat and polished with various grades of SiC paper and finished with 1 µm Al oxide paste.

The Bernex CVD coatings were produced by IonBond AG, Switzerland. The CVD process is to place the sample to be coated in a furnace at a selected temperature and to introduce a gas mixture. Given the composition of the gas and the temperature in the furnace, the coating formed is the most thermodynamically stable compound. The coating thickness depends on the time in the furnace. This can be predicted from known growth rates and can typically be controlled to within ±15% across the sample. The conditions and gases used are described in Table 1.

The sputter-coated samples were prepared by M. Fassone, European Organisation for Nuclear Research, CERN, Switzerland using unbalanced magnetron sputtering. The first two were hard coatings: TiAlN and CrN. A low deposition temperature (150 °C) was used to increase hardness and reduce internal stress. The third coating was a new style wear-resistant coating, MoS<sub>2</sub>+Ti. The substrates were spring steel and were fully formed furnace springs. They therefore had to be pressed flat before GD-OES analysis and, because of their complex shape, the coatings were not of uniform thickness. These samples had been characterised previously by EDX, X-ray diffraction (XRD), X-ray photoelectron spectroscopy (XPS) and GD-OES.<sup>23</sup>

The GD-OES analysis was conducted using a JY 5000 RF instrument, manufactured by Jobin-Yvon Horiba (JY), Longjumeau, France. This instrument is equipped with a standard 4 mm JY glow discharge source, two optical spectrometers (a polychromator and a monochromator) and Quantum 2000 V1.02 software. The source can be operated with constant pressure monitored in the source and constant power from the rf generator. The source conditions, chosen to give a flat crater shape in the coatings, were 700 Pa and 35 W. In addition the instrument is equipped with a matching box, used to balance the impedance between the rf generator and the GD source, that also provides continuous monitoring of the dc bias voltage.

The software allows the combination of bulk and coated samples in the same calibration by allowing the operator to switch between automatic and manual selection of the integration time. All the results shown here were obtained with the same calibration. The argon flush time, *i.e.*, the time between mounting the sample and the application of the rf power, was 60 s for all samples. For the bulk samples, using the automatic setting, the pre-integration (also called pre-burn) time was 240 s and the integration time 15 s, with three replicates. For the coated samples, an integration time of 240 s

was used and the data range was chosen manually from the resulting intensity–time curves, avoiding the non-uniform regions, *i.e.*, the intensities in the first seconds and in approaching the coating/substrate interface. In this way the recorded intensities for the coated sample represented an average for the coating. The emission lines used on the polychromator were (wavelengths in nm): Al 396.15, C 156.14, Cr 425.43, Fe 371.99, H 121.56, Mo 386.41, N 149.26, S 180.73 and Ti 337.27.

Sputtering rates, crater shapes, crater depths and coating thicknesses were all measured using a UBM profilometer equipped with a 2 µm point diamond stylus. Unfortunately, such measurements are typically accurate only to about ±10% because of variations in sample flatness, crater shape and crater roughness.

## Theory

Calibration in GD-OES is often based on the following calibration function,<sup>24</sup> in second order:

$$c_i(q_M/q_{Ref}) = k_i^{(1)} R_i I_i + k_i^{(2)} (R_i I_i)^2 + b_i \quad (1)$$

where  $c_i$  is the concentration of element  $i$ ,  $(q_M/q_{Ref})$  is the relative sputtering rate of the material compared to a reference material (both in mass per unit area per s),  $k_i^{(1)}$  and  $k_i^{(2)}$  are constants,  $R_i$  the inverse relative emission yield,  $I_i$  the intensity, and  $b_i$  the background signal. During calibration,  $c_i$  is known *a priori*,  $(q_M/q_{Ref})$  is measured separately,  $k_i^{(1)}$ ,  $k_i^{(2)}$  and  $b_i$  are determined by regression, which leaves  $R_i$  to be determined.

Note: many authors prefer to combine  $k_i^{(1)} R_i$  into a single parameter, often given the same symbol  $R_i$ . Keeping the two parameters separate has several advantages; most notably,  $R_i$  includes only relative changes, while the absolute part is taken up by the constant  $k_i^{(1)}$ . If the reader prefers to use a single parameter for  $R_i$  then a constant must be included in the following expressions for  $R_i$ .

## Dc bias voltage

Several approaches to determining values for  $R_i$  have been tried previously. A common practice is to choose plasma conditions that minimise any changes in  $R_i$  and then assume it is unchanged, *i.e.*, assume  $R_i = 1$ .<sup>25,26</sup> Another approach is to choose samples in the calibration that have similar matrices to the unknown samples to be analysed.<sup>24</sup> In this way the values for  $R_i$  will be similar for the known and unknown samples and so can be assumed to be accounted for in the values for  $k_i^{(1)}$ ,  $k_i^{(2)}$  and  $b_i$ . This approach is usually called ‘matrix-matching’, and is a common approach used in many analytical techniques. A third approach is to parameterise  $R_i$  in terms of externally measured plasma parameters, such as source current,  $I_g$ , voltage,  $V_g$  and pressure  $p_g$ , and then to correct  $R_i$  for any changes in these parameters. One form of this approach developed by Payling and based on earlier work by Bengtson<sup>27,28</sup> is given by

$$R_i = I_g^a (V_g - V_0)^b p_g^c \quad (2)$$

where  $V_0$ ,  $a$ ,  $b$  and  $c$  are constants.

When conditions are kept constant in calibration and analysis, usually only one of these parameters is allowed to

**Table 1** Conditions used to produce CVD coatings

Coating	Gas	Temperature/°C
TiN	Ti tetrachloride in N <sub>2</sub> and H <sub>2</sub> carrier gas	950
TiC	Ti tetrachloride in methane and H <sub>2</sub> carrier gas	1000
TiCN	Ti tetrachloride in acetyl nitryle (CH <sub>3</sub> CN) and H <sub>2</sub> carrier gas	850
Cr <sub>7</sub> C <sub>3</sub>	Chromium dichloride over C-containing steel in Ar and H <sub>2</sub> carrier gas	1000

vary and so  $R_i$  can be expressed as a function of this single parameter. When the source is operated with constant pressure and applied power, the parameter that changes is the source impedance determined by the nature of the sample matrix, in particular by the secondary electron emission of the sample.<sup>29</sup> In going from one material to the next, if the electron emission yield increases, the current will increase and, at constant power, the voltage will decrease. This change can be represented by the dc bias voltage,  $V_{dc}$ , and it will vary roughly as the square of  $V_{dc}$ . Hence, at constant pressure, the inverse relative emission yield can be represented by a function of  $V_{dc}$ , where

$$R_i \approx (V_{dc} - V_0)^{2b} \quad (3)$$

Since we are only interested in a relatively small range of values of  $V_{dc}$ , e.g., 450 V to 900 V, this function can be simplified to the linear equation

$$R_i \approx 1 + r_i(V_{dc} - V') \quad (4)$$

where  $r_i$  is a fitting parameter and  $V'$  is a reference voltage, e.g., 700 V, chosen to be somewhere in the normal range of this parameter.

### Hydrogen effect

Recently another effect on emission yield has been reported, a hydrogen effect. Small amounts of hydrogen in the plasma, either from contamination of the plasma gas (argon) or by sputtering from the sample, can affect the measured intensities of the analytes. The effect is to increase the intensity of some lines from the analyte elements while decreasing the intensities of other lines from these same elements. Hydrogen also affects the background signal by the formation of molecular species, such as hydrides and molecular hydrogen, in the plasma. We will not consider the effect on the background further here but concentrate on the apparent changes to emission yield, since these changes if uncorrected will have a major effect on calibration curves and the accuracy of analysis.

Hodoroaba *et al.* have measured the changes in intensity of a number of emission lines as a function of the amount of hydrogen in the plasma.<sup>22</sup> We have taken their results and normalised them so that we could explore the general form of the effect on the inverse relative emission yield. For emission lines that increase with hydrogen content, we divided the intensities by the value at zero hydrogen and then normalised the intensities to have the same average slope. The result is shown in Fig. 1(a). For emission lines that decrease with hydrogen content, we again divided the intensities by the value at zero hydrogen but then plotted the inverse intensities, normalised to have the same average slope. The result is shown in Fig. 1(b). The general trend of these results is that the effect of hydrogen on the inverse relative emission yield can be described by either of the following:

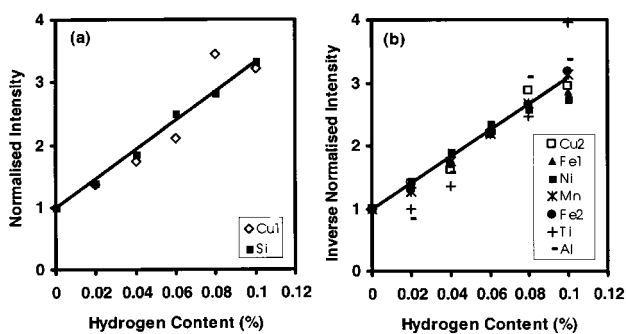


Fig. 1 Changes to intensity with hydrogen content in the plasma, normalised to 1 for zero hydrogen and to the same average slope: (a) intensities and (b) inverse intensities. Data from Hodoroaba *et al.*<sup>22</sup>

$$R_i \approx 1/(1 + h_i I_H) \quad (5)$$

and

$$R_i \approx 1 + h_i I_H \quad (6)$$

where  $I_H$  is the hydrogen intensity, and eqns. (5) and (6) refer to lines whose intensities increase or decrease with hydrogen, respectively. Remember that  $R_i$  here is the inverse relative emission yield. More complex functions could be used to improve the fit in both Fig. 1(a) and (b), such as a third order polynomial or a logistic 'S' curve, but more work is required before such complex functions are justified and can be used to improve the quantitative analysis.

### Combined correction

In general, when operating at constant pressure and power, the inverse relative emission yield may vary with both the dc bias voltage and the hydrogen content. Hence we have the combined effect

$$R_i \approx \{1 + r_i(V_{dc} - V')\} / \{1 + h_i I_H\} \quad (7)$$

and

$$R_i \approx \{1 + r_i(V_{dc} - V')\} \times \{1 + h_i I_H\} \quad (8)$$

again depending on whether the effect of hydrogen is to increase or decrease intensities, respectively.

### Results

Table 2 shows the relative sputtering rates and dc bias voltages measured for each calibration sample. The sputtering rates in the nitride and carbide coatings and the pressed TiN powder sample were typically much slower, by about a factor of five, than sputtering rates in the bulk metal samples.

Eqs. (7) and (8) were combined with eq. (1) to form a calibration function, and values for the various constants were determined by regression. Typical values for  $r_i$  in eq. (4) for all elemental lines were around 0.002, giving the average inverse relative emission yields shown in the Table. The inverse relative emission yields varied by about 30% over the range of samples.

The hydrogen effect was determined from the calibration curves for Fe 371.99 and Cr 425.43 to have  $h_i$  values of approximately 1.0 and 1.5, respectively. The comparable values obtained from the results of Hodoroaba *et al.*,<sup>22</sup> who added known percentages of hydrogen to the argon plasma, were 14 and 38, respectively. The ratio of their numbers to ours is an average of 20. This suggests that a typical hydrogen signal of 0.3 V in the calibration corresponds to about 0.015% (*i.e.*, 0.3/20) hydrogen in the plasma. The factor 0.3/20 comes from the equality  $h_i I_H \approx h_{Hod} I_{Hod} \approx 20 h_i I_{Hod}$ , where  $I_{Hod}$  is the quantity

Table 2 Dc bias voltages and average inverse relative emission yields obtained for the calibration samples

Sample	Relative sputtering rate <sup>a</sup>	Dc bias/V	$R_i$ (average)
1265a	1.00	651	0.90
JK41-1N	0.83	641	0.88
SS487/1	1.39	674	0.95
1203	1.49	710	1.02
BS80D	1.39	662	0.92
1169	1.39	652	0.90
550/3	0.28	586	0.77
TiN powder <sup>b</sup>	0.26	589	0.78
TiN	0.20	600	0.80
TiC	0.20	562	0.72
TiCN	0.20	560	0.72
Cr <sub>7</sub> C <sub>3</sub>	0.57	689	0.98

<sup>a</sup>Relative to nearly pure iron sample 1265a, whose sputtering rate was 0.419 g m<sup>-2</sup> s<sup>-1</sup> (3.2 μm min<sup>-1</sup>). <sup>b</sup>Pressed.

**Table 3** Hydrogen effect on the emission lines

Line	Effect <sup>a</sup>	$h_i$
N 149.26	+++	6.5
C 156.14	+	1.2
S 180.73	++	3.0
Ti 337.27	-	0.30
Fe 371.99	--	0.75 <sup>b</sup>
Mo 386.41	-	0.14 <sup>b</sup>
Al 396.15	-	0.20 <sup>b</sup>
Cr 425.43	---	1.75 <sup>b</sup>

<sup>a</sup> '+' means increases intensity and '-' means decreases intensity; the more symbols the greater the effect. <sup>b</sup> Values obtained from the analysis of data from Hodoroaba *et al.*<sup>22</sup> divided by 20; i.e., scaled for the hydrogen signal.

of hydrogen used by Hodoroaba *et al.* This allows us to use other values from Hodoroaba *et al.*, after scaling; notably values for Mo 386.41 and Al 396.15. Other values were determined from the calibration curves. Table 3 shows that the values for parameter  $h_i$  vary significantly from line to line. The effect of hydrogen on intensities is to increase N 149.26, C 156.14 and S 180.73 and decrease Ti 337.27, Fe 371.99, Mo 386.41, Al 396.15 and Cr 425.43.

Calibration curves are shown for C 156.14 and Cr 425.43 in Figs. 2 and 3, respectively. The curves for C 156.14 show the effects of dc bias voltage correction alone and combined dc bias voltage and a positive hydrogen correction. The dc bias correction improves the calibration curve for C 156.14 significantly, as does the hydrogen correction, which brings one datum point otherwise far too high in intensity back onto the calibration curve. One of the best measures of the quality of a calibration curve is the standard error of estimate (SEE).<sup>30</sup> The values for SEE are shown in Table 4. The error is greatly reduced using both corrections. Since there was little change in the dc bias voltage for the Cr-containing calibration samples, the curves for Cr 425.43 show mainly the effect of the hydrogen correction in bringing one datum point far too low in intensity onto the calibration curve.

The qualitative depth profile obtained for the TiCN coated steel calibration sample is shown in Fig. 4. Though the coating is well defined, in that there is good depth resolution between the coating and substrate, the intensities appear to vary throughout the coating; in particular the nitrogen intensity appears much stronger closer to the surface and the titanium signal weaker. The Fe signal rises rapidly at the interface between the coating and substrate indicating good depth resolution. Also shown is the dc bias voltage ( $V_{dc}$ ), which is significantly lower in the coating than in the substrate.

The quantitative depth profiles for this sample are shown in Fig. 5(a) without correction, and (b) with combined dc bias and hydrogen corrections. The concentrations are presented in Atomic%, rather than the more common Mass%, to emphasise the stoichiometry. The results in Fig. 5 demonstrate the effectiveness of both the dc bias correction and the hydrogen

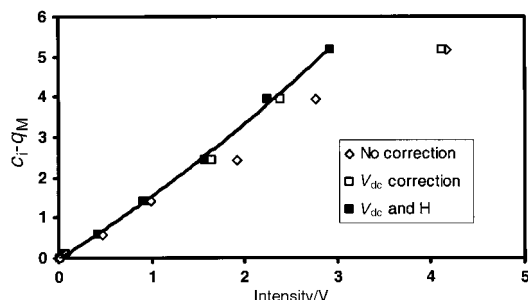


**Fig. 2** Calibration curve for C 156.14: (◇) no correction, (□) with  $V_{dc}$  correction, and (■) with both  $V_{dc}$  and hydrogen corrections.

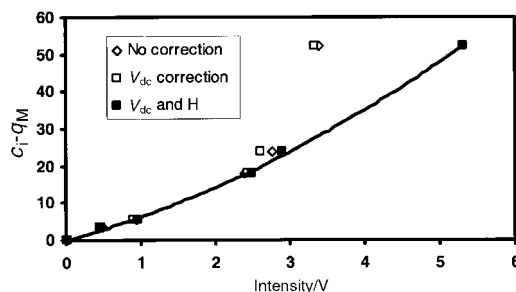


**Fig. 3** Calibration curve for Cr 425.43: (◇) no correction, (□) with  $V_{dc}$  correction, and (■) with both  $V_{dc}$  and hydrogen corrections.

**Table 4** Standard error of estimate for the calibration curves shown in Figs. 2 and 3. The smaller the number the better the fit

Line	No correction	Both $V_{dc}$ and H corrections
C 156.14	0.16	0.07
Cr 425.43	7.2	0.6

correction. Except for a thin layer of carbon contamination on the immediate surface, the fully corrected results show the coating is of uniform and stoichiometric composition. Also notable is a TiN intermediate layer.

Figs. 6 to 8 show the quantitative depth profiles of the other three coated calibration samples, after combined dc bias voltage and hydrogen corrections. The coatings all appear to have near uniform and stoichiometric compositions. The surface carbon is residual contamination and is typical of such coatings.<sup>1</sup> The depth profile for the TiN coating is similar to that obtained by Schultz *et al.*,<sup>15</sup> who fortunately did not need to include a hydrogen correction as their coating was produced by PVD in a pure argon atmosphere. While Schultz *et al.* used a Ti intermediate layer, here a TiCN layer is present.

The quantitative depth profiles of the sputter-coated samples are shown in Figs. 9 to 11. While these are thinner and less uniform, both in thickness and composition, than the CVD samples, the GD-OES analysis shows they have compositions in general agreement with the EDX/XRD analysis. The

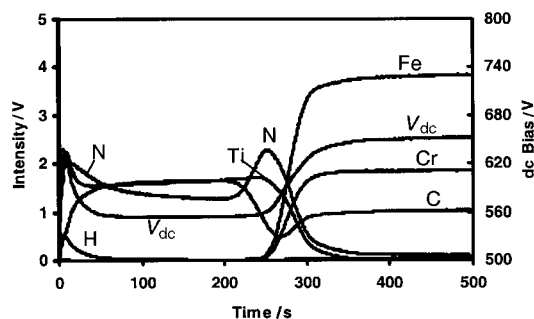


**Fig. 4** Qualitative depth profile of TiCN coated steel.

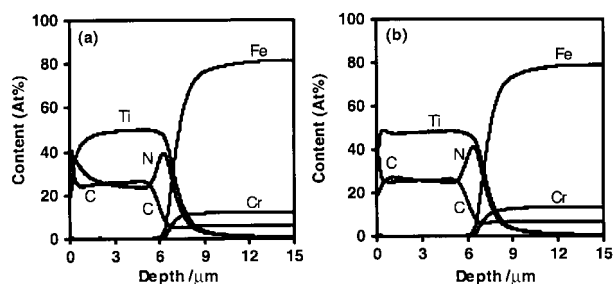


**Fig. 5** Quantitative depth profile of TiCN coated steel: (a) no correction and (b) with both  $V_{dc}$  and hydrogen corrections.

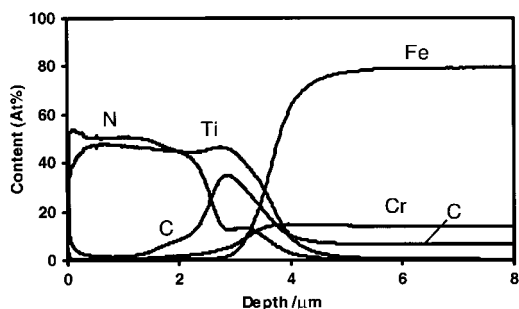


Fig. 6 Quantitative depth profile of TiN coated steel, with both  $V_{dc}$  and hydrogen corrections.

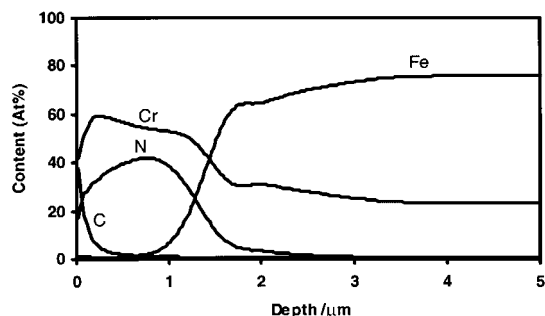


Fig. 10 Quantitative depth profile of CrN coated steel, with both  $V_{dc}$  and hydrogen corrections.

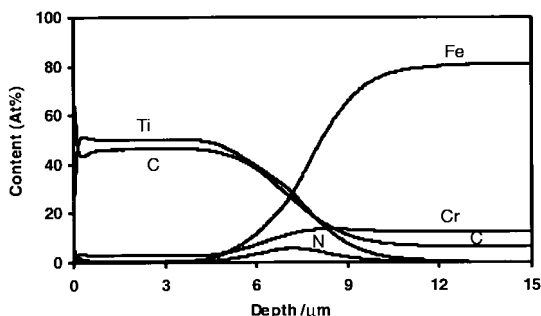


Fig. 7 Quantitative depth profile of TiC coated steel, with both  $V_{dc}$  and hydrogen corrections.

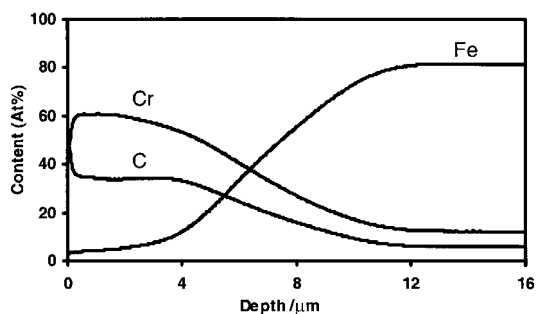


Fig. 8 Quantitative depth profile of  $Cr_7C_3$  coated steel, with both  $V_{dc}$  and hydrogen corrections.

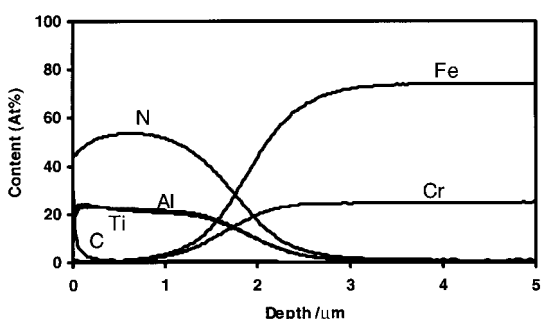


Fig. 9 Quantitative depth profile of TiAlN coated steel, with both  $V_{dc}$  and hydrogen corrections.

MoS+Ti coating varied in thickness over the sample with an obvious difference in colour, being much darker in the thicker areas. GD-OES results for two different areas are shown in Fig. 11(a) and (b). The GD-OES results show that there is not only a difference in thickness but also in composition, with the thinner area having a higher S to Mo ratio.

After each measurement the depth of the resulting crater was measured and compared with the total depth in the quantitative depth profile. These are shown in Table 5. For the CrN coating the sputtering was also stopped at the point

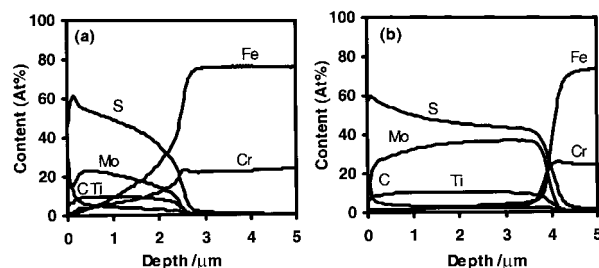


Fig. 11 Quantitative depth profile of  $MoS_2$ +Ticoated steel, with both  $V_{dc}$  and hydrogen corrections; (a) and (b) are two different locations on the sample.

where the nitrogen signal dropped to half its value in the coating as a way of measuring the coating thickness. This result is also shown in Table 5.

The stoichiometries of the coatings, as determined by GD-OES using the combined dc bias voltage and hydrogen corrections, are shown in Table 6. They agree well with those expected from the thermodynamics for the CVD coatings and from the EDX/XRD analyses of the PVD coatings. A wide range of possible stoichiometries was determined by EDX and XRD and these are reflected in the ranges shown for the final three coatings in Table 6; see, for example CrN, where the Cr/N ratio could vary by a factor of 2. Some of this apparent variation is due to the different thicknesses of the coatings,

Table 5 Crater depths and coating thicknesses calculated from quantitative depth profiles and measured craters

Sample	Calculated depth/ $\mu m$	Measured depth/ $\mu m$
TiN crater	16.4	15.1
TiC crater	21.4	20.9
TiCN crater	21.0	20.8
$Cr_7C_3$ crater	21.9	22.3
TiAlN crater	6.4	7.6 <sup>a</sup>
CrN coating	1.4	1.5 <sup>a</sup>
CrN crater	6.7	$\approx 10^a$
$MoS_2$ +Ticrater	9.3	8.3 <sup>a</sup>

<sup>a</sup>Samples are not flat so it is difficult to measure crater depth accurately.

Table 6 Dominant stoichiometry in coatings

Sample	Expected	Found
TiN	$Ti_1 N_1^a$	$Ti_1 N_1$
TiC	$Ti_1 C_1^a$	$Ti_1 C_1$
TiCN	$Ti_1 C_{1-1.2} N_{0.8-1}^a$	$Ti_1 C_1 N_1$
$Cr_7C_3$	$Cr_7 C_3^a$	$Cr_6 C_3$
TiAlN	$Ti_{0.8-1} Al_{0.9-2} N_2^b$	$Ti_1 Al_1 N_2$
CrN	$Cr_{1-2} N_1^b$	$Cr_{1.4} N_1$
$MoS_2$ +Ti	$Mo_1 S_2 + Ti_{0.5-1}^b$	$Mo_1 S_{1.6-2.5} + Ti_{0.3-0.5}$

<sup>a</sup>From thermodynamics. <sup>b</sup>Measured by EDX and XRD.

which would have affected the analytical results from the different techniques as each is most sensitive to a different depth. EDX takes most of its signal from the first 0.5–1  $\mu\text{m}$ , while XRD senses several  $\mu\text{m}$ , depending on the energies chosen. From EDX, the three coatings contained  $\text{TiAl}_{1.2}\text{N}_{2.6}$ ,  $\text{CrN}$  and  $\text{MoS}_2 + \text{Ti}_{0.5}$  phases, respectively, while, from XRD, the coatings contained  $\text{Ti}_3\text{Al}_2\text{N}_2$ ,  $\text{Cr}_2\text{N}$  and  $\text{MoS}_2 + \text{Ti}$  phases, respectively. The GD-OES results are within these values.

## Discussion and conclusions

The results present demonstrate that rf-GD-OES can now provide quantitative depth profiles of hard coatings, giving correct composition and thickness, even in the presence of hydrogen. The near uniform stoichiometric composition of the CVD coatings indicates that such coatings are useful in the calibration of GD-OES.

The magnitude of the hydrogen effect, and, in particular, the values for the parameter  $h_i$  can be determined by regression during the calibration. But this requires calibration samples with and without hydrogen and such samples are generally not available. Fortunately, as shown, these values may also be determined independently of the calibration. First, data are collected for all the elemental lines of interest following the procedure described by Hodoroaba *et al.*, *i.e.*, by leaking known amounts of hydrogen into the plasma. Then the results are converted to  $h_i$  values as described in the Theory section above. Finally the  $h_i$  values are scaled to relate the measured hydrogen intensities to the hydrogen content in the plasma. At least one calibration sample containing hydrogen is required to do this. This sample can then be used later for recalibration (drift correction).

## Acknowledgements

The authors thank IonBond AG, Switzerland for providing the Bernex CVD coatings, Dr M. Fassone, CERN, Switzerland for providing the PVD coatings, and Dr Johann Michler, EMPA, Switzerland for his helpful comments on the manuscript. RP thanks EMPA for their kind invitation to work on this project, and their warm welcome and support during the project. The work was supported financially by BBW (Bundesamt für Bildung und Wissenschaft), Switzerland.

## References

- 1 S. Anderbouhr, V. Ghetta, E. Blanquet, C. Chabrol, F. Schuster, C. Bernard and R. Madar, *Surf. Coat. Technol.*, 1999, **115**, 103.

- 2 D. L. Smith, *Thin Film Deposition: principles and practice*, McGraw Hill, New York, 1995.
- 3 D. Delfosse and M. Aeberhard, *Oberflächen-Polysurfaces*, 1997, (7), 7.
- 4 D. Delfosse, M. Aeberhard and S. Sgobba, *Oberflächen-Polysurfaces*, 1998, (1), 24.
- 5 R. Payling, D. G. Jones and A. Bengtson, *Glow Discharge Optical Emission Spectrometry*, John Wiley, Chichester, 1997.
- 6 H. Hocquaux, L. Ohannessian, Y. Flandin-Rey and J. Chapon, UNIREC, Firminy, France, *Rept. No. 1609*, 1984.
- 7 H.-R. Stock and P. Mayr, *Härterei-Tech. Mitteilungen*, 1986, **41**, 145.
- 8 H. Böhm in *Glow Discharge Optical Emission Spectrometry*, ed. R. Payling, D. G. Jones and A. Bengtson, John Wiley, Chichester, 1997, pp. 676–687.
- 9 F. L. Freire Jr., L. F. Senna, C. A. Achete and T. Hirsch, *Nucl. Instrum. Meth. Phys. Res. B*, 1998, **136**(8), 788.
- 10 L. F. Senna, C. A. Achete, T. Hirsch and F. L. Freire Jr., *Surf. Coat. Technol.*, 1997, **94**(5), 390.
- 11 A. Kirsten, C. Pietzsch and H. Oettel, *Fresenius' J. Anal. Chem.*, 1998, **26**, 834.
- 12 D.-F. Lii, J.-L. Huang and M.-H. Lin, *Surf. Coat. Technol.*, 1998, **99**, 197.
- 13 I. J. Smith, D. Gillibrand, J. S. Brooks, W.-D. Münz, S. Harvey and R. Goodwin, *Surf. Coat. Technol.*, 1997, **90**, 164.
- 14 C. Rebholz, H. Ziegele, A. A. Voevodin, J. M. Schneider and A. Matthews, *Surf. Eng.*, 1997, **13**, 375.
- 15 A. Schulz, H.-R. Stock, P. Mayr, J. Staevs and D. Schmoekkel, *Surf. Coat. Technol.*, 1997, **94**(5), 446.
- 16 O. Wänstrand, M. Larsson and P. Hedenqvist, *Surf. Coat. Technol.*, 1999, **111**, 247.
- 17 Z. Weiss and K. Marshall, *Thin Solut. Films*, 1997, **308**(9), 382.
- 18 O. Wänstrand, R. Fella and N. Axén, *Surf. Coat. Technol.*, 1997, **94**(5), 469.
- 19 O. Wänstrand, M. Larsson and P. Hedenqvist, *Surf. Coat. Technol.*, 1999, **111**, 247.
- 20 A. Bengtson and S. Hånström, in *Proceedings of Fifth Internal Conf. on Prog. Anal. Chem. in Steel Metals Industries*, ed. R. Tomellini, European Commun., Luxembourg, 1999, pp. 47–54.
- 21 V.-D. Hodoroaba, V. Hoffmann, E. B. M. Steers and K. Wetzig, *J. Anal. At. Spectrom.*, 2000, **15**, 951.
- 22 V.-D. Hodoroaba, V. Hoffmann, E. B. M. Steers and K. Wetzig, *J. Anal. At. Spectrom.*, 2000, **15**, 1075.
- 23 M. Fassone, CERN Rpt. 99/10/19 1999.
- 24 R. Payling, *Spectroscopy*, 1999, **13**, 36.
- 25 K. Marshall, *J. Anal. At. Spectrom.*, 1999, **14**, 923.
- 26 A. Bengtson and S. Hånström, *J. Anal. At. Spectrom.*, 1998, **13**, 437.
- 27 R. Payling, *Surf. Interface Anal.*, 1995, **23**, 12.
- 28 A. Bengtson and M. Lundholm, *J. Anal. At. Spectrom.*, 1988, **3**, 879.
- 29 R. Payling, 2000. [www.thespectroscopynet.com/techniques/secondary\\_ey.htm](http://www.thespectroscopynet.com/techniques/secondary_ey.htm)
- 30 R. Payling, in *Glow Discharge Optical Emission Spectrometry*, ed. R. Payling, D. G. Jones and A. Bengtson, John Wiley, Chichester, 1997, pp. 428–439.